Synthesis and Structural Characterization of ZnTe/ZnSe Core/Shell Tunable Quantum Dots

by

Juan Guan

B. S. Chemistry

University of Science and Technology of China, 2006

Submitted to the Department of Chemistry

in Partial Fulfillment of the Requirements for the Degree of

Master of Science in Chemistry

at the

MASSACHUSETTS INSTITUTE OF TECHNOLOGY

February 2008

Signature of the Author_____

Department of Chemistry

January 3, 2008

Certified by_____

Moungi G. Bawendi

Professor of Chemistry

Thesis Supervisor

Accepted by _____

Robert W. Field

Chairman, Departmental Committee on Graduate Students

For Family and Friends.

Synthesis and Structural Characterization of ZnTe/ZnSe Core/Shell Tunable Quantum Dots

by

Juan Guan

Submitted to the Department of Chemistry on January 3, 2008 in Partial Fulfillment of the Requirements for the Degree of Master of Science in Chemistry

Abstract

Colloidal semiconductor nanocrystals or quantum dots have attracted much attention recently with their unique optical properties. Here we present a novel approach to synthesize ZnTe/ZnSe core/shell tunable quantum dots. Characterizations such as transmission electron microscopy, wavelength dispersive X-ray spectroscopy, powder x-ray diffraction are employed to give evidence for the core/shell structure. Absorption, and photoluminescence spectra demonstrate the tunability of this ZnTe/ZnSe core/shell system, and fluorescence lifetime decays suggest a core/shell structure is made.

Thesis Supervisor: Moungi G. Bawendi, PhD

Title: Professor of Chemistry

Table of Contents

List of Figures

Chapter 1

General Introduction

1.1 Quantum Confinement and Optical Properties

Colloidal semiconductor nanocrystals or quantum dots (QDs) have attracted much attention recently with their unique properties such as their size-tunable emission, their continuous absorption profile to the blue of the band edge, and their stability against photobleaching. These properties grant QDs promising applications in optoelectronics and biology.[1-3] A quantum dot is a semiconductor core surrounded by a layer of organic ligands (figure 1.1). The smallest QDs (< 1 nm in diameters) are nearly molecular (<100 atoms) whereas the largest QDs (>20 nm in size) can be composed of 100,000 atoms. An example of the stacking of atoms in a QD is provided (figure 1.2). The optical properties of QDs evolve dramatically with their size, an effect known as quantum confinement. Figure 1.3 illustrates the effect of quantum confinement on electronic states going from 3D bulk materials to 0D quantum dots. This size dependent effect was firstly observed on 2D thin films of semiconductor materials (quantum wells) grown by molecular beam epitaxy.[4, 5] The thickness of the thin film is comparable to the Bohr radius of the exciton so that the exciton is confined, which modifies the density of states such that there are fewer band edge states and the bandgap is shifted to the blue. Later studies led to 1D quantum wires/rods and 0D quantum dots. As the size of a QD is smaller than the material's Bohr exciton radius, the dimensions of the crystal become so small that the photoexcited carriers feel the boundary, causing the continuous density of states in the

bulk to collapse into discrete electronic states. QDs are considered "artificial atoms" for precisely this reason. After a series of approximations, the quantum dot problem can be reduced to the "Particle-In-a-Sphere" model. From this model, it is easy to deduce that the more confined the carriers are, the higher the bandgap energy is, and correspondingly the potential photoluminescence should blue-shift. A scheme is shown in Figure 1.4 to illustrate the principle of size-dependent tunability. Figure 1.5 demonstrates the tunability of absorption in the well-established CdSe quantum dot system. As the size becomes bigger, the first absorption feature red-shifts. Note that the corresponding PL follows the same trend in emission peak positions. The entire PL is largely tuned in the visible window.

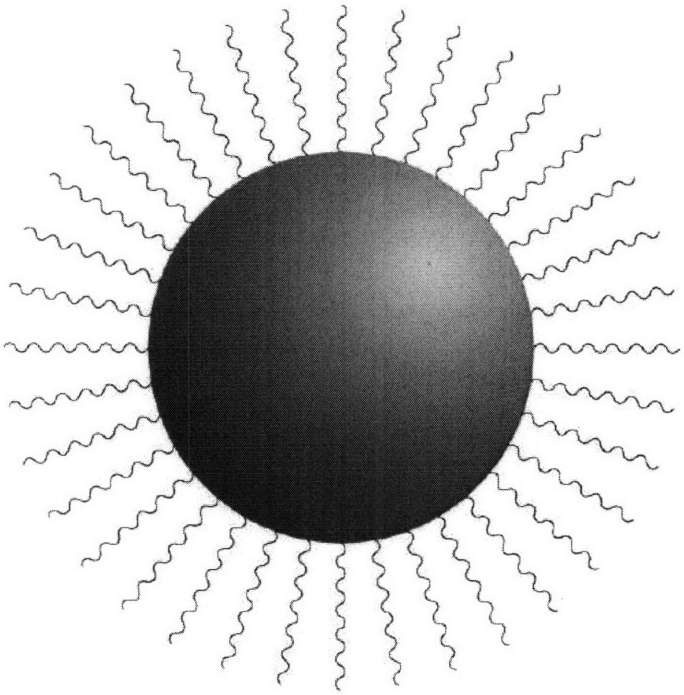

Figure 1.1 Cartoon of a colloidal quantum dot with a semiconductor nanocrystal core and a passivating organic ligand shell. The core size usually ranges from 2-15 nm. Adapted from Yen, B. K. Ph. D. Thesis, Massachusetts Institute of Technology, Cambridge, MA, 2007.

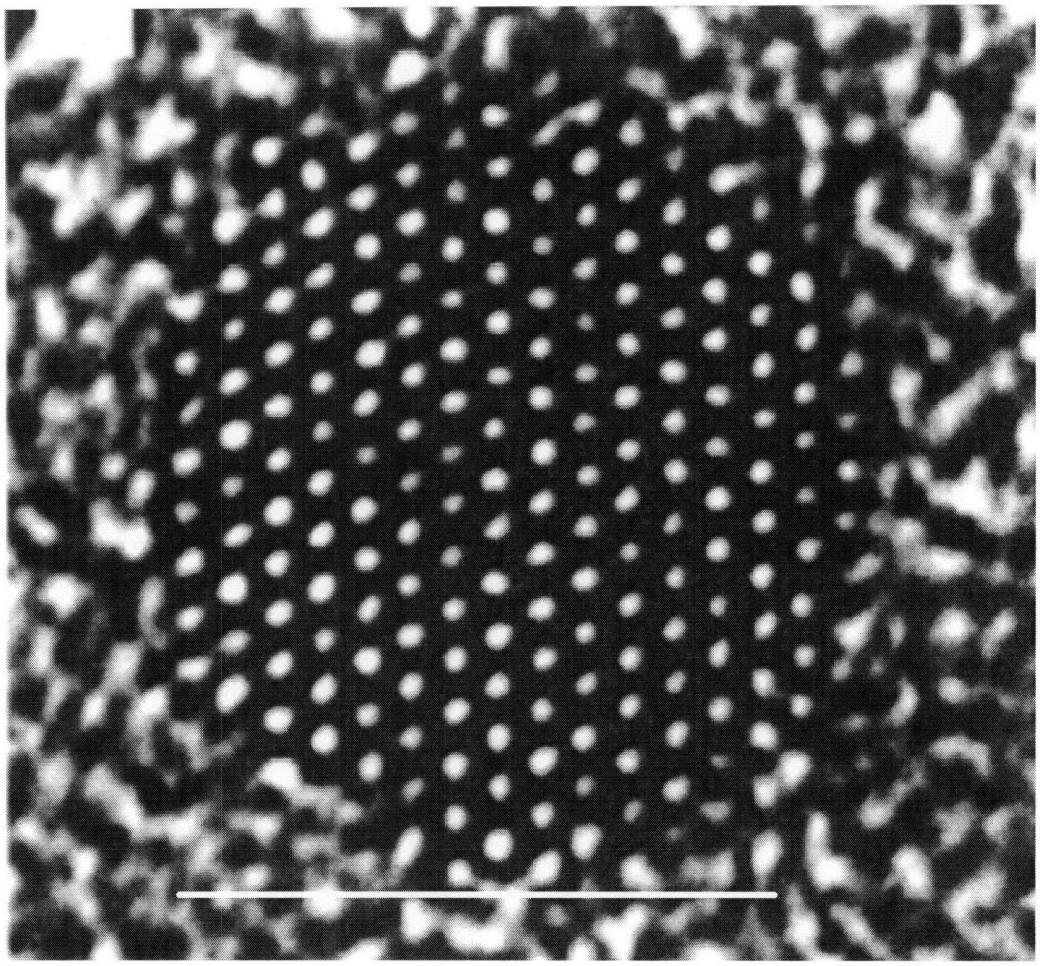

Figure 1.2 High-resolution transmission electron microscope image of a CdSe nanocrystal. The actual array of atoms can be seen (Adapted from J. J. Shiang, A. V. Kadavanich, R. K. Grubbs, and A. P. Alivisatos, *J. Phys. Chem.* volume 99, page 17417, 1995).

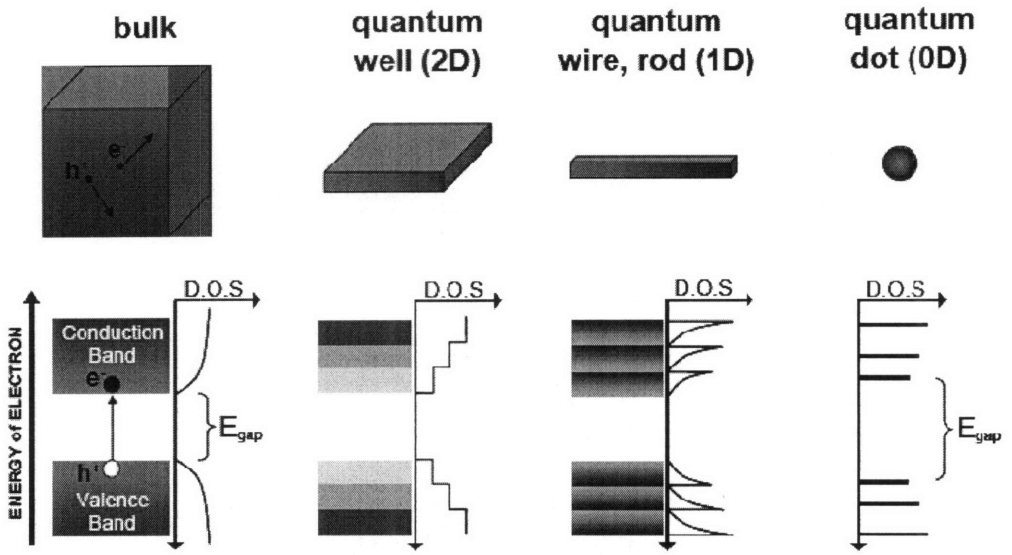

Figure 1.3 Illustration of quantum confinement going from 3D bulk semiconductor to 2D quantum wells to 1D quantum wires/rods and finally to 0D quantum dots, which are quantum confined in all three dimensions and atomic like states result. Adapted from Steckel, J. Ph. D. Thesis, Massachusetts Institute of Technology, Cambridge, MA, 2006.

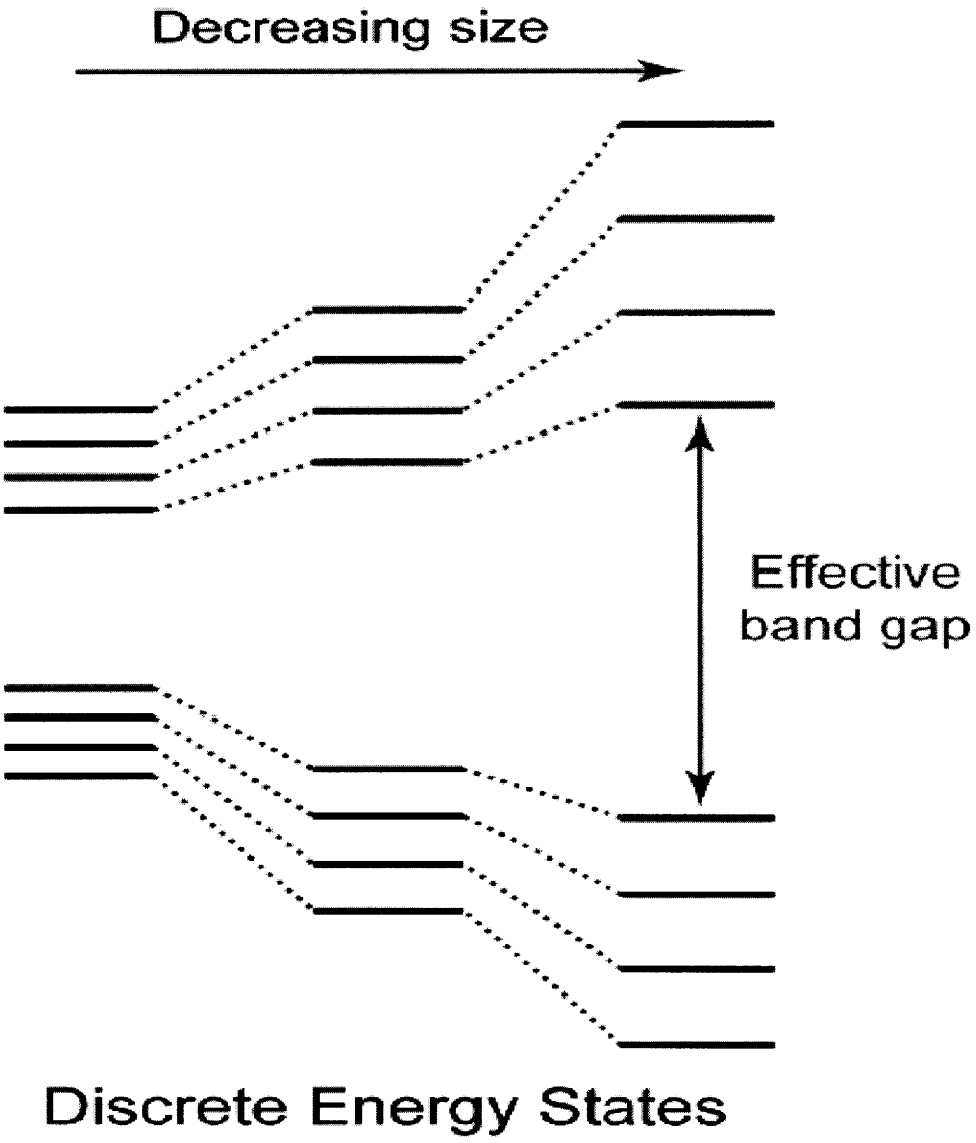

Figure 1.4 Schematic depiction of the size-tunability principle for quantum dots. The splitting of states increases as the size decreases. Adapted from Yen, B. Ph. D. Thesis, Massachusetts Institute of Technology, Cambridge, MA, 2007.

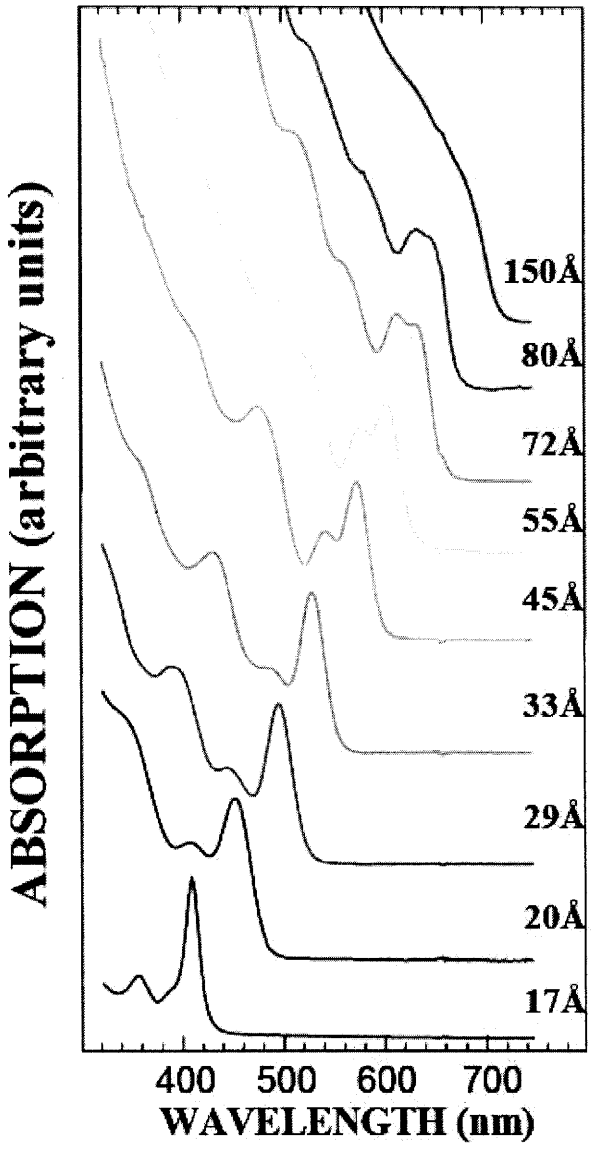

Figure 1.5 Absorption spectra for a size series of CdSe nanocrystals ranging from 2 to 15 nm in diameter.

1.2 Review of Quantum Dot Preparations

Recently the "hot-injection" method is widely applied in QD synthesis. A batch of QDs is prepared by rapidly injecting precursors into a hot solvent and organic ligand

system. The relatively high temperature (~300 ℃) ensures the decomposition of precursors to form monomers, resulting in a burst in nucleation followed by a slower growth on the existing nuclei as the concentration of monomers decreases rapidly and the reactivity of the monomers is lower since a lower temperature is set for the growth. High temperature annealing is also found to contribute to the removal of surface trap states. With fewer surface trap states, the photoexcited carriers are less likely to fall into trap states and have a higher possibility to take part in radiative recombination. Consequently, PL intensity can be enhanced. A typical reaction set-up is shown in figure 1.6.

To achieve monodisperse nanocrystals, the growth kinetics is studied. The classic nucleation and growth model can be applied to quantum dot colloidal synthesis. Generally speaking, the formation of NCs can be divided into three stages. First, the precursors quickly decompose to form reactive monomers. The monomer concentration continues to increase until a critical supersaturation occurs which induces energetic nucleation. This nucleation burst lowers the monomer concentration and partially relieves the supersaturation. Meanwhile, the still high concentration ensures NC growth onto the existing nuclei. Within a certain range, the growth is in the size focusing region as smaller particles need less material to grow a shell whereas larger particles need more materials to achieve a shell of the same thickness. When monomer concentration is extremely low, as will surely happen when monomers are depleted from the reaction, Oswald ripening happens. Small particles dissolve to compensate the growth of large particles. At this point, the QD growth enters into the de-focusing region. In order to make high-quality, monodisperse samples, QD growth is strategically controlled in the

growth-focusing region, by controlling the amount of precursors, the growth time, and multiple injections to keep concentrations of monomers relatively high.

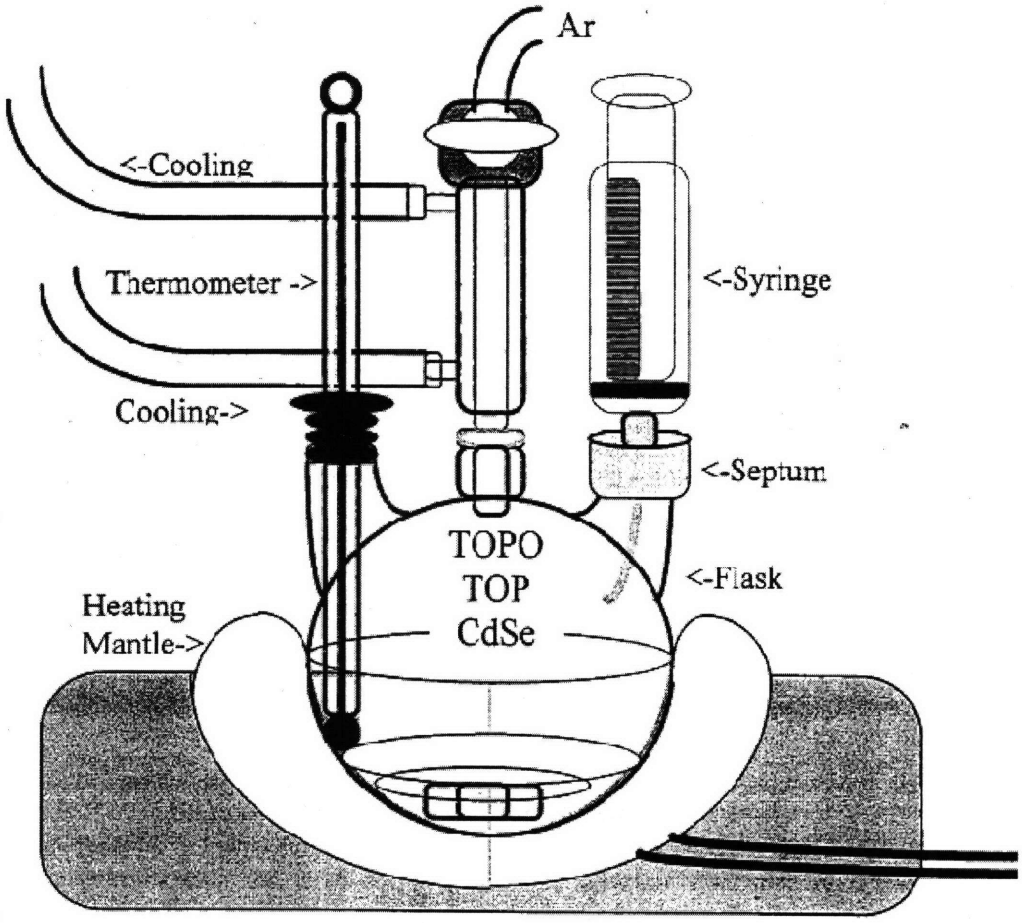

Figure 1.6 Cartoon of a typical hot-injection set-up for CdSe quantum dot synthesis. Precursor solution is swiftly injected into a three-neck-flask containing hot Solvent / organic ligand system. Adapted from Murray, C. Thesis, Massachusetts Institute of Technology, Cambridge, MA, 1995.

As the size of quantum dots is so small (2-15 nm), the surface to volume ratio is high. Thus the properties of the surface play an important role in the quality of QD samples. In particular, surface defects are known to trap photoexcited carriers.[6] To achieve high quantum efficiency, various surface passivation schemes are used. First of

all, long annealing times are found to be helpful in enhancing PL intensity. We speculate that annealing results in the rearranging of semiconductor material and organic ligands at the surface which leads to a decreased number of surface trap sites. Consequently, carriers are less likely to fall into those trap sites and more likely to undergo radiative recombination. Second of all, inorganic shells are sometimes overcoated onto the existing nanocrystal cores. This is found to passivate the surface and increase quantum efficiency. Note that this inorganic shell process is particularly important for the fabrication of quantum dot light emitting devices (QD-LEDs).

Separation of QDs from their original growth solution is often necessary for future process. The established technique commonly used is repeated solvent/nonsolvent extraction. Typically, addition of methanol induced flocculation of nanocrystals and butanol was added to help mix the methanol and growth solution. Precipitated nanocrystals were separated from the supernatant by centrifugation and redispersed in hexane. Ethanol is found to be gentler than methanol, and therefore used when nanocrystals lose fluorescence from the harsh purification from methanol. Acetone, an alternative to methanol, is found to remove certain salts that methanol cannot remove. This purification procedure is also used in size-selective precipitation, by gently adding a limited amount of nonsolvent (methanol in most cases). Large particles precipitate first, and thus nanocrystals can be roughly separated by their sizes.

1.3 References

[1] F. Chen, D. Gerion, *Nano Lett.* **2004**, 4, 1827.
[2] F. Fleischhaker, R. Zentel, *Chem. Mater.* **2005**, 17, 1346.
[3] H. Huang, A. Dorn, G. Nair, V. Bulovic, M. Bawendi, *Nano Lett.* **2007**, 7, 3781.
[4] D. Chemla, *Physics Today* **1993**, 46.

[5] D. Chemla, D. Miller, *J. Opt. Soc. Am. 2* **1985**, 1155.
[6] P. Guyot-Sionnest, M. Hines, *Appl. Phys. Lett.* **1998**, 72, 686.

Chapter 2

Synthesis of ZnTe/ZnSe Core/Shell Quantum Dots

2.1 Type II Quantum Dots

In type-I core/shell structures the bandgap of the shell material is larger than that of the core. The conduction and valence band offsets are such that the conduction band of the shell is of higher energy than that of the core, while the valence band of the shell is of lower energy than that of the core. This leads to an effective confinement of electrons and holes in the core material. In type-II core/shell QDs, both the conduction and valence bands of the core are lower in energy (or higher) than those of the shell, consequently, one carrier is mostly confined to the core, while the other is mostly confined to the shell. Recently, Kim et al. have reported the synthesis of CdTe/CdSe and CdSe/ZnTe type-II heterostructures.[1] Absorption and emission wavelengths in the near-IR were observed, which would not have been accessible with a single material. In addition, owing to slow electron–hole recombination, extraordinarily long radiative lifetimes have been found. Spatial separation of charge carriers might render type-II quantum dots suitable for photovoltaic or photoconduction applications in which one of the carriers is injected from the QDs into the matrix before recombination can occur. Interesting new bandgap possibilities arise from engineering bandgaps between different materials to form type-II quantum dots.

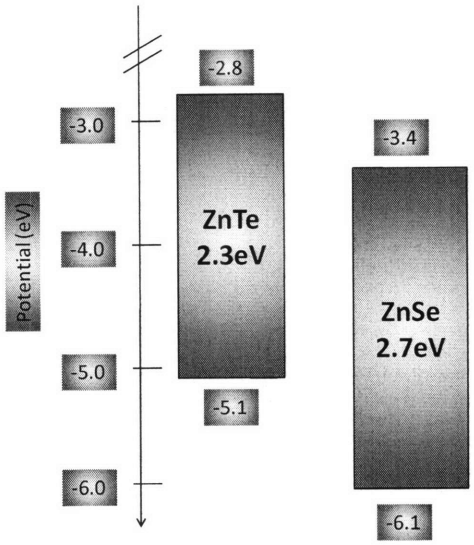

Figure 2.1 Bulk conduction and valence band diagram of ZnTe and ZnSe semiconductors.

2.2 Possibility of ZnTe/ZnSe type-II Quantum Dots

Figure 2.1 shows the band offsets for ZnTe and ZnSe bulk semiconductor materials. It can be predicted from the diagram that in type II ZnTe/ZnSe core/shell QDs, electrons should mainly be confined in the ZnSe shell whereas holes should mostly be located in the ZnTe core. The recombination process involves electrons from the conduction band in ZnSe and holes from the valence band in ZnTe, resulting in a smaller energy bandgap than that of either ZnTe or ZnSe. In particular, the conduction band offset of ZnSe (-3.4 eV) and the valence band offset of ZnTe (-5.1 eV) leads to a projected bulk bandgap value of 1.7 eV for ZnTe/ZnSe core/shell type II QDs. Due to quantum confinement, these novel ZnTe/ZnSe core/shell QDs can be potentially tuned to

emit at energies greater than 1.7 eV, much like CdSe, whose bulk band gap is also 1.7 eV.[2]

2.3 Experimental

2.3.1 Chemicals

1-octadecene (ODE, 90%) was purchased from Sigma Aldrich. Oleylamine (OA, 80%-90%) was purchased from Acros Organics. Zinc acetate (99.6%) was purchased from Mallinckrodt. Selenium powder (99.999%) and oleic acid (95%) were purchased from Alfa. Di-ethyl-zinc ($ZnEt_2$), tri-octyl-phosphine (TOP, 97%) and tellurium powder (22 mesh) were purchased from Strem.

2.3.2 Stock Solutions

To prepare 0.1M zinc oleate solution as a shell precursor, 0.46 g zinc acetate was mixed with 6.2 g oleic acid and 22.8 g ODE. The mixture was thoroughly degassed and then heated up to 240°C until a clear yellow solution resulted. The solution was allowed to cool down to room temperature and reheated until clear when in later use. 0.1M TOPSe and TOPTe stock solutions were prepared by dissolving Se and Te powder respectively in TOP at room temperature.

2.3.3 Synthesis of ZnTe/ZnSe Core/Shell QDs

All the operations were carried out using standard air free techniques unless stated otherwise. Typically, a mixture of OA (0.8 g) and ODE (3 g) was put in a 50ml three-neck-flask and heated to 110 ℃ to degas for 1 hr. 12 mg $ZnEt_2$ and 1 ml TOPTe was swiftly injected into the flask at 285 ℃. The nanocrystals were allowed to grow at 270 ℃

for 2 min. The solution was kept at 240 ℃ for shell growth. The zinc precursor and the selenium precursor were alternatively added into the flask, allowing 20 min between each precursor to complete the reaction. The Te center-doped ZnSe dots (an extremely small ZnTe core and thick ZnSe shell) were synthesized by substituting part of the tellurium precursor with the selenium precursor and performing a co-injection under the same reaction conditions as for the ZnTe core synthesis.

2.4 Results and Discussions

2.4.1 Choices of Materials

$ZnEt_2$ is much more reactive than other zinc sources, such as zinc acetate and zinc oxide. Therefore, $ZnEt_2$ can be reduced more easily to zinc atoms to form free zinc atoms. Previous experiments employing zinc acetate or zinc stearate did not produce high quality quantum dots. It is reported elsewhere that high quality ZnSe or ZnS QDs are synthesized from zinc carboxyl precursors.[3] However, we could not reproduce that protocol.

Oleylamine seems exchangeable with octadecylamine, as the PL properties with these two amines are similar to one another. We favor oleylamine as a liquid precursor is easier to handle and potentially can be used in a microfluidic system without much modification to the recipe. Amines are an important type of ligand, and appear irreplaceable. In control experiment, we explore other ligand system, such as using phosphines (TOP), and we could not produce high quality colloidal quantum dots.

Zinc oleate is critical in terms of the photoluminescence of this system. It is worth noting that no fluorescence is seen from bare ZnTe cores (sometimes a broad PL to

the red of the ZnTe bulk bandgap is seen and is attributed to deep trap emission) while slight addition of zinc oleate induces bright band-edge emission. We ascribe this to the gentle etching and modification of the surface by zinc oleate which results in a decreasing number of surface traps. Consequently, the photoexcited carriers are less likely to fall into those trap states and have a higher probability to undergo radiative recombination.

2.4.2 Successive Ion Layer Absorption and Reaction (SILAR)

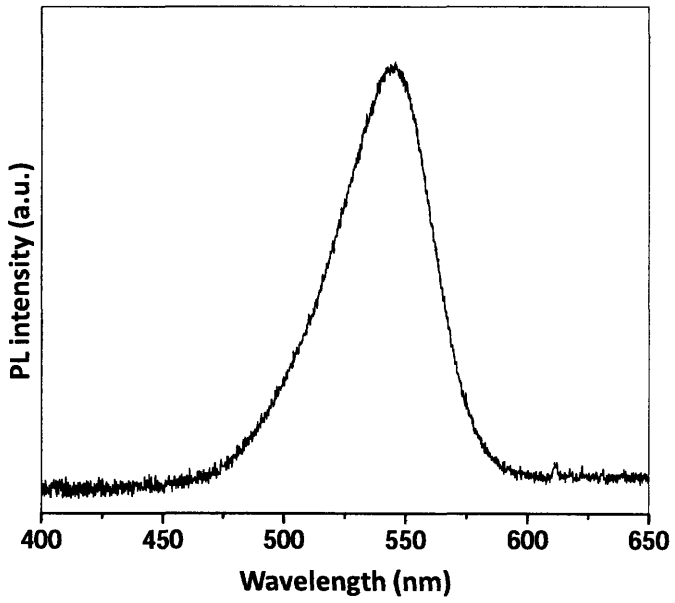

Figure 2.2 Typical photoluminescence spectrum from non-SILAR method. Usually the emission peak shape from non-SILAR method is asymmetric.

A mother batch of ZnTe core growth solution was separated into different flasks. To each flask, various amounts of ZnSe shell material were added using the method of successive ion layer absorption and reaction (SILAR).[4, 5] In a typical SILAR shell growth procedure, zinc precursor corresponding to one hypothetical monolayer is first

added dropwise, and after sufficient annealing the same amount of selenium precursor is added to form another hypothetical monolayer. The process is repeated in order to grow a successively thicker ZnSe shell. The purpose of SILAR shell growth is mainly three fold. First, it prevents independent nucleation of the shell material, in this case, the formation of separate ZnSe nanocrystals. Second, the annealing in between alternative shell materials (zinc and selenium precursors) allows sufficient time for one material to react so that the chemical composition of the shell is not biased towards either material. Third, the slow addition keeps precursor concentrations low and favors isotropic and uniform growth that results in spherical dots and symmetric photoluminescence (PL) spectra. In our experiments, a non-SILAR method (simultaneous addition of zinc and selenium precursors) almost always gives asymmetric spectra with a long tail into the bluer region than the PL maximal wavelength (see Figure 2.2).

2.4.3. Other reaction conditions

The high temperature for shell growth is not only helpful for uniform growth but also necessary to activate the inert zinc oleate precursor. In this protocol, we needed temperatures above 230 °C for QDs to exhibit PL.

Long annealing times allow materials to react completely and facilitate rearrangement of the dot surface to minimize surface defects so that the PL intensity is enhanced.

2.5 Conclusions

ZnTe/ZnSe core/shell quantum dots are synthesized in one-pot using the SILAR method. This successfully incorporates tellurium into the ZnSe system. The choices of

materials, the reaction conditions, and the advantages of the SILAR method are thoroughly discussed above.

2.6 References

[1] S. Kim, B. Fisher, H.-J. Eisler, M. Bawendi, *J. Am. Chem. Soc.* **2003**, 125, 11466.
[2] C. Murray, D. Norris, M. Bawendi, *J. Am. Chem. Soc.* **1993**, 115, 8706.
[3] L. Li, N. Pradhan, Y. Yang, X. Peng, *Nano Lett.* **2004**, 4, 2261.
[4] R. Xie, U. Kolb, J. Li, T. Basche, A. Mews, *J. Am. Chem. Soc.* **2005**, 127, 7480.
[5] J. Li, Y. Wang, W. Guo, J. Keay, T. D. Mishima, M. Johnson, X. Peng, *J. Am. Chem. Soc.* **2003**, 125, 12567.

Chapter 3

Characterization

3.1 Transmission Electron Microscopy

3.1.1 Introduction

Transmission electron microscopy is an irreplaceable tool to characterize the structure of nanocrystals. Lattice image contrast and Z contrast provide complimentary information. Lattice imaging probes the crystalline core of particles with planes oriented perpendicular to the electron beam; Z contrast refers to the diffuse scattering of the electron beam being proportional to the atomic number (Z) of the element, and Z contrast provides contrast in the disordered / misoriented regions.

3.1.2 Experimental

To analyze size and size distribution transmission electron microscopy (TEM) was performed. Aliquots were taken from the growth solution. Addition of methanol induced flocculation of nanocrystals and butanol was added to help mix methanol and the growth solution. Precipitated nanocrystals were separated from the supernatant by centrifugation and redispersed in hexane. This nanocrystal solution was drop cast onto copper grids with carbon support by slow evaporation of solvent in air at room temperature. TEM images were acquired using a JEOL 200CX operating at an acceleration voltage of 200kV.

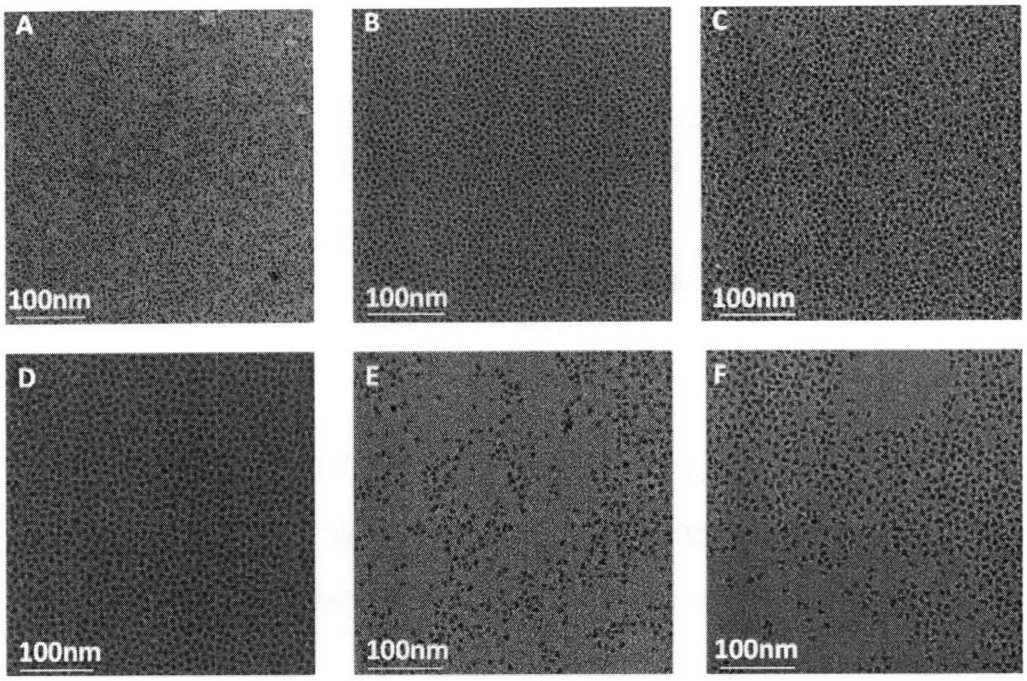

Figure 3.1 Transmission electron microscope images of ZnTe core and ZnTe/ZnSe core/shell QDs with varying shell thicknesses. A) ZnTe QDs with a diameter of 4.4 nm. The shell thickness increases from B to F. B-D) ZnTe/ZnSe core/shell QDs with diameters of 5.2±0.5 nm, 5.2±0.6 nm, and 5.7±0.7 nm respectively. E) A mixture of spherical ZnTe/ZnSe core/shell QDs with particle size of 6.5±0.6 nm and prism-shaped QDs with long axis of 9.2±0.9 nm and short axis of 5.8±0.7 nm. F) Prism-shaped QDs with a long axis of 8.7±0.9 nm and a short axis of 5.97±0.8 nm.

3.1.3 Results and Discussions

Figure 3.1 presents transmission electron microscopy (TEM) images of ZnTe core and ZnTe/ZnSe core/shell QDs of different shell thicknesses. Figure 3.1A shows ZnTe cores of an average diameter of 4.4 nm with a size distribution of 13%. The average size and size distribution are obtained by measuring 100 QDs in each sample. See Figure 3.2. The ZnTe core growth is not a rapid process in the current reaction condition, which provides control over the average core size. Figure 3.1B-F demonstrates the size evolution and shape evolution of ZnTe/ZnSe core/shell nanocrystals with increasing

ZnSe shell materials and the QDs in Figure 3.1B-D are largely spherical. The QD size changes from 4.4 nm (bare ZnTe core) to 5.7 nm while the size distribution remains roughly at 13%. Figure 3.1E shows a mixture of spherical QDs (6.5 nm) and prism-shaped QDs with long and short axis. These prismatic QDs dominate when more ZnSe shell material is added (Figure 3.1F).

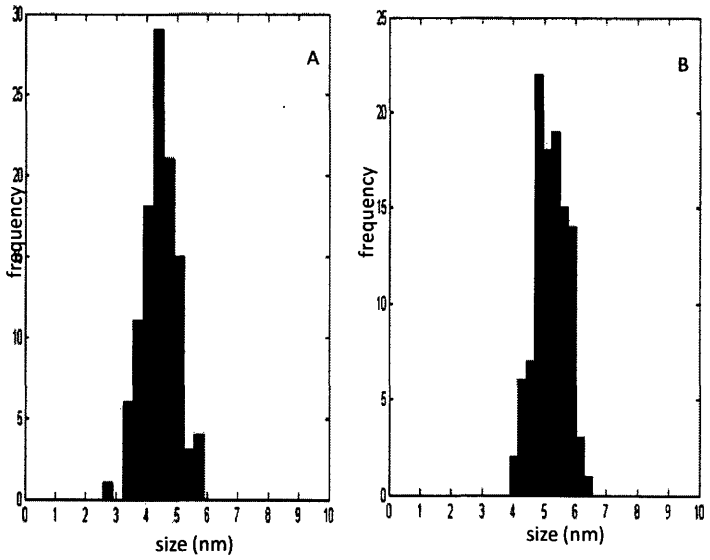

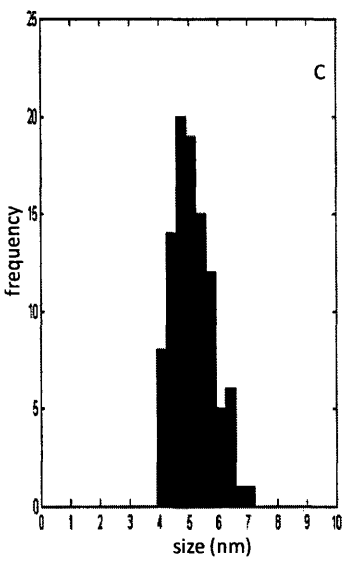
C
frequency
size (nm)

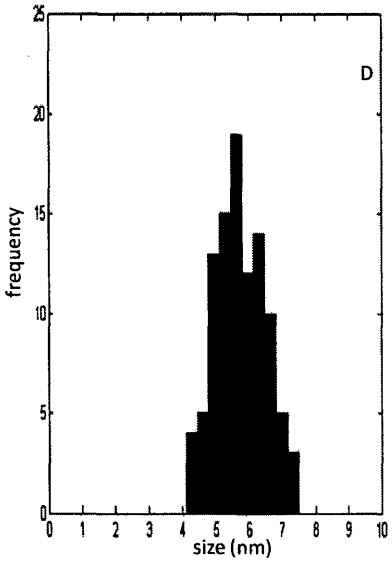
D
frequency
size (nm)

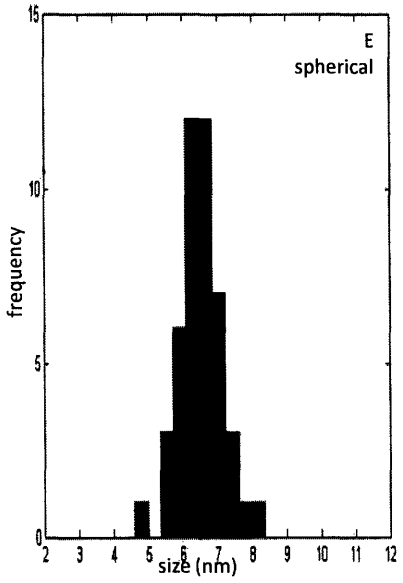
E
spherical
frequency
size (nm)

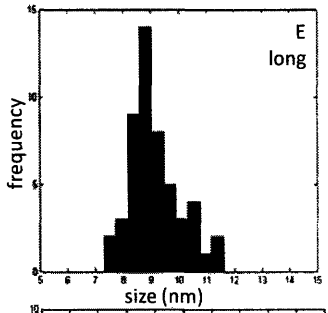
E
long
frequency
size (nm)

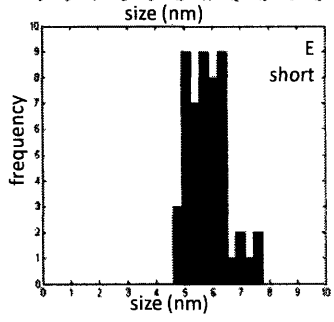
E
short
frequency
size (nm)

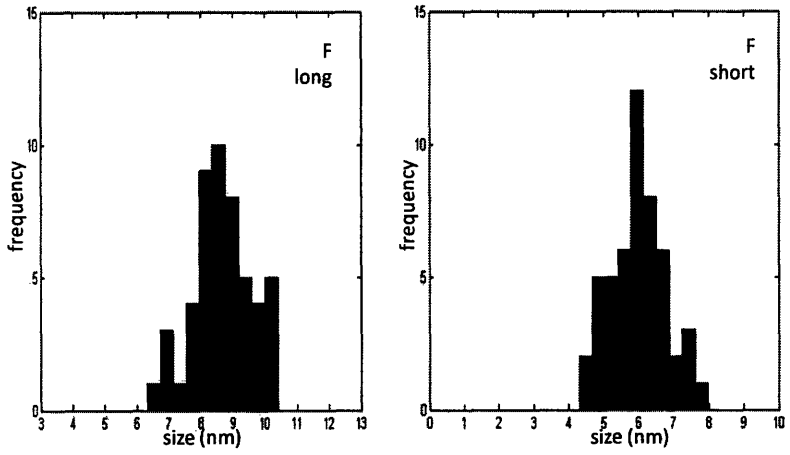

Figure 3.2 Histograms from statistics of each TEM images in Figure 3.1. The average size and size distribution is done by sampling 100 QDs for each sample.

3.2 Wavelength Dispersive X-ray Spectroscopy

3.2.1 Introduction

Wavelength Dispersive X-ray Spectroscopy (WDS) is a technique used in elemental analysis. High energy electrons are focused onto the specimen and X-rays are produced due to energy loss from inelastic collisions between electrons. Each element's characteristic X-ray has a distinct wavelength, which requires adjusting the tilt of the crystal in the spectrometer at a specific angle to properly diffract the X-ray. WDS generally requires element be known and by counting the number of X-rays of a specific wavelength, the atomic composition of the specimen can be probed.

3.2.2 Experimental

Elemental composition data was obtained from Wavelength dispersive X-ray spectroscopy (WDS) on a JOEL JXA-733 Superprobe. Methanol extraction and centrifugation was repeated three times. Concentrated hexane solutions were drop cast onto Si (100) wafers to form thick films of nanocrystals and solvent was allowed to evaporate completely.

3.2.3 Results and Discussions

Wavelength dispersive X-ray spectroscopy (WDS) was performed to determine the elemental composition of this series of QD samples. Table 1 reveals how the composition changes with increasing shell thickness. With increasing shell thickness from A to F, the number of selenium atoms gradually and steadily increases from 0% to 43% of the total number of atoms. Consequently, tellurium drops from 47% to 9% in atomic composition, further demonstrating that the ZnSe shell is added onto the existing bare ZnTe core. When we assume a ZnTe/ZnSe core/shell spherical structure with a perfectly defined ZnTe/ZnSe interface and with each material retaining its own lattice structure, the expected particle size can be calculated from relative selenium and tellurium amounts. The corresponding sizes measured from TEM are listed for comparison. For spherical QDs, the actual sizes are consistent with theoretical sizes within the range of experimental error. This consistency supports that ZnTe/ZnSe core/shell QDs are synthesized over a wide range of shell thicknesses.

	Zn%	Se%	Te%	expected size (nm)	actual size (nm)
A	53	0	47	---	4.4
B	53	17	30	5.1	5.2
C	55	22	23	5.3	5.2
D	51	29	20	5.7	5.7
E	47	40	13	6.7	6.5[a]
F	48	43	9	7.4	---[b]

Table 1 The first three columns show elemental composition of ZnTe core and ZnTe/ZnSe core/shell QDs of different shell thickness measured by wavelength dispersive X-ray spectroscopy. Samples A-F correspond to the same A-F as in Figure 3.1. The column showing expected size refers to size computed from the observed Se and Te composition assuming spherical core/shell and the bulk lattice structure, as described in the text. The actual size measured using TEM agrees within experimental uncertainty.

[a] Sample E is a mixture of spherical QDs of 6.5 nm and prism-shaped QDs. [b] As sample F was mainly prism-shaped QDs, the actual size of the hypothetical spherical counterpart lacked physical sense to consider and was not computed.

In all samples in this series, the number of zinc atoms consistently comprises of about 50% of the total number of atoms. This is expected as the ZnTe core and the ZnSe shell both have a 1:1 cation:anion ratio even though the zinc precursors are different for core ($ZnEt_2$) and shell (zinc oleate) growth. However, it is worth noting that the zinc shell precursor (zinc oleate) is the limiting factor and the system has the tendency to become selenium-rich. The high temperature and long time annealing between addition of alternative shell materials (zinc and selenium precursors) allows sufficient time for one

material to react so that the chemical composition of the shell is not biased towards either zinc or selenium material. On the other hand, there is a slight trend of zinc percentage dropping from sample A to F which suggests that the reactivity of zinc precursor is still limiting and the surface of the nanocrystals becomes slightly selenium-rich. The irregular shapes with thicker shells may partially stem from this imbalance in chemical composition.

3.3 Powder X-ray Diffraction

3.3.1 Introduction

X-ray scattering techniques reveal information about the crystallographic structure of materials and thin films. These techniques are based on observing the scattered intensity of an x-ray beam hitting a sample as a function of incident and scattered angle, polarization, and wavelength or energy. Powder X-ray diffraction (PXRD) is a technique used to characterize the crystallographic structure, crystallite size (grain size), and preferred orientation in polycrystalline or powdered solid samples. Powder diffraction is commonly used to identify unknown substances.

3.3.2 Experimental

Powder X-ray diffraction (PXRD) spectra were collected on a Rigaku Ru300 X-ray diffractometer operating at 50 kV and 300 mA. Samples for PXRD were prepared from filtering through a 0.02 um syringe filter and five-time methanol extraction to remove excessive organic impurity and the concentrated hexane solutions (QDs in 3 ml growth solution were redispersed into 0.3 ml hexane) were drop cast onto a zero

background scattering Si plate to form thick (~0.5 mm) films of nanocrystals. Samples were measured in a 2Θ range from 15 to 60 degree.

3.3.3 Results and Discussions

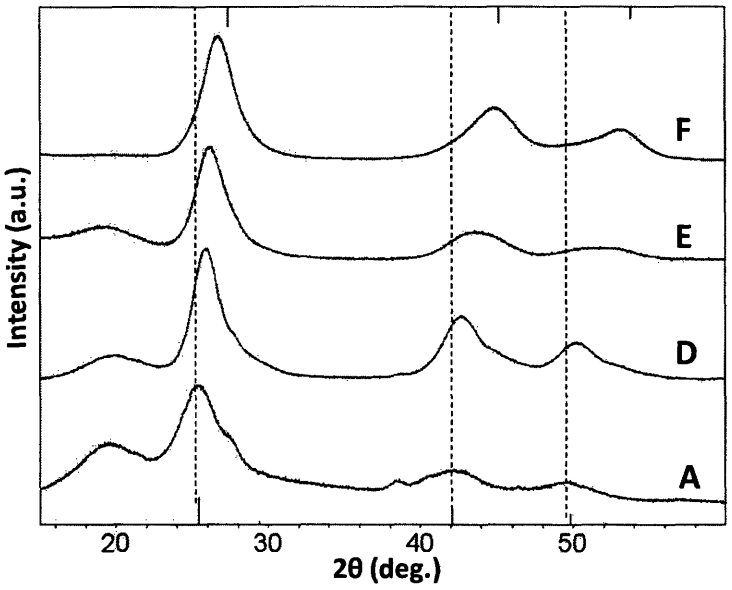

Figure 3.3 X-ray diffraction patterns of ZnTe QDs and ZnTe/ZnSe core/shell QDs with different shell thickness. The labels parallel those of the samples in Figure 3.1. For reference, the marks on the bottom abscissa show the XRD peaks characteristic of bulk ZnTe (zinc blende). The marks on the top abscissa show the XRD peaks characteristic of bulk ZnSe (zinc blende).

Powder X-ray diffraction was used to determine the crystallographic properties of the core/shell structures (Figure 3.3). As the shell thickness increases, the diffraction peak position successively shifted from ZnTe (zinc blende) towards ZnSe (zinc blende). While small nanocrystals give broad peaks in XRD patterns and therefore peaks are harder to resolve than those of bulk materials, the high growth temperature (270 ℃ for

core and 240 ℃ for shell) ensures crystallinity of these nanoparticles. Note that no separate ZnSe nanocrystals are observed in XRD patterns, suggesting that the SILAR method can suppress nucleation during shell growth. Finally, we attribute the broad peaks centered around 20 degrees to organic residuals in the sample, as the same peaks were observed for a control sample containing only the solvent system without nanocrystals.

3.4 Absorption and Photoluminescence

3.4.1 Experimental

UV-Vis absorption and photoluminescence were measured on a Hewlett Packard 8453 spectrophotometer and an Ocean Optics USB4000 spectrometer.

3.4.2 Results and Discussions

We next demonstrated the absorption and corresponding photoluminescence (PL) tunability for this series of ZnTe/ZnSe core/shell QDs. The band edge absorption feature is discernable up to 4 MLs of ZnSe (e in Figure 3.4A) while the feature diminishes with increasing shell thickness (f, g in Figure 3.4A). This is consistent with theoretical prediction that type-II QDs have small absorbance near the band edge as spatial separation of charge carriers leads to a decreased wave function overlap and thus a weak oscillator strength.[1] The band edge absorption feature of the ZnTe/ZnSe core/shell QDs red shifts from 420 nm (bare ZnTe core) to 515 nm (ZnTe core with 4 MLs of ZnSe shell) as the shell grows thicker. Correspondingly, the PL of these ZnTe/ZnSe core/shell QDs can range anywhere from 500 nm to 590 nm. When the shell thickness is less than 4 MLs, the typical Quantum Yield (QY) is 15%. It is interesting to note that initially synthesized ZnTe cores exhibit no fluorescence, and that slight addition of zinc oleate

shell precursor solution at high temperature gives rise to bright band edge photoluminescence. We speculate that zinc oleate gently etches and therefore modifies the surface so that the number of surface trap sites decreases. Consequently, charge carriers are less likely to fall into trap states and have a higher probability of radiative recombination. After overcoating with various thicknesses of ZnSe, these QDs have a full width at half maximum (FWHM) of 25-35 nm when the emission wavelength is shorter than 550 nm. A FWHM of less than 45 nm is obtained for redder QDs even when TEM images revealed that QD shapes become more irregular. In this core/shell model system, we only varied the shell thickness to achieve spectral tunability. It is expected that the emission profile can be further red-shifted beyond 590 nm using larger ZnTe cores having thick ZnSe shells.[2] Future experiments will be done to confirm this prediction.

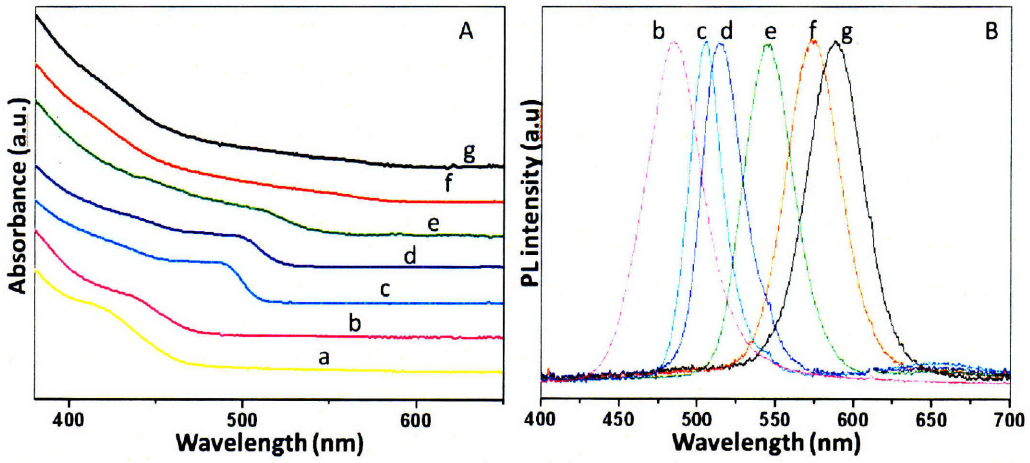

Figure 3.4 A) UV-Vis absorption spectra of QDs formed by in this study. a) ZnTe bare cores, 4.4 nm diameter. b) ZnTe/ZnSe QDs formed by co-injection as described in the text. c-g) Spectra of ZnTe/ZnSe core/shell with the same 4.4 nm core and different shell thickness. Spectra (c-g) correspond to samples B-F in Figure 3.1. B) Normalized room temperature photoluminescence of ZnTe/ZnSe core/shell QDs. PL spectra (b-g) correspond to absorption spectra in (A).

There is also a possibility to make alloyed instead of the proposed core/shell structures under the following reaction conditions: (1) high reaction temperatures (~240 C), which increases mobility of the atoms, and (2) long annealing times between monolayers, which gives atoms time to diffuse. Also, due to the nature of the one-pot synthesis, the tellurium atoms left from the core growth can grow into the shell. For $ZnSe_{1-x}Te_x$ alloys in bulk, the bandgap evolution with composition exhibits a bowing with the lowest point at $ZnSe_{0.35}Te_{0.65}$ and two endpoints with higher bandgap values for pure ZnTe and ZnSe.[3] In the synthesis we start from a ZnTe core and gradually add a ZnSe shell. If alloying is occurring in this system, one would expect to see an initial red-shift followed by a blue-shift as the composition of the nanocrystals goes from pure ZnTe towards increasing ZnSe composition. However, as we add ZnSe shell precursors on ZnTe cores of a certain size, these QDs have only a red shift (from 500 nm to 590 nm) in PL peak position and blue-shifting is never observed even after the composition becomes dominant in ZnSe (F in Table 1). In addition, the lowest bandgap achievable for an alloyed structure in the bulk is 590 nm. It is expected that with quantum confinement effects, the alloy model cannot red-shift the PL of QDs to 590 nm as we observe here with ZnTe/ZnSe core/shell structures.

The PL from ZnTe/ZnSe core/shell QDs is quenched in air within a few minutes even with thick ZnSe shells, whereas they are stable if kept under inert atmosphere, which allows them to be potentially used in quantum dot light emitting devices (QD-LEDs) where the QDs are isolated from the atmosphere.[4] In addition, compared to the size of green CdSe QDs (~3 nm in diameter), our green QDs are larger (>5nm in diameter), which may lead to more efficient QD-LEDs due to their larger absorption

cross sections.[5] The air-stability can be improved by first removing excess tellurium via precipitation and centrifugation under inert atomosphere, and then overcoating a protective layer (such as ZnSe or ZnS) on the existing core/shell structure.[6, 7] These overcoated dot solutions are stable in air for months. Note that the second ZnS (or ZnSe) shell improved air-stability, but did not increase QY. We attribute the poor air stability to the oxidation of tellurium,[8] which creates trap sites on the QD surface, whereas the removal of excess tellurium minimizes the chance of it being incorporated during shell growth, and the new protective shell layer acts as a barrier for the diffusion of oxygen into the nanocrystal.

To access the PL spectral window below 500 nm, an extremely small ZnTe core was attempted in an alternative synthesis. The PL from b in Figure 3.4B corresponds to nanocrystals made by co-injection of zinc, tellurium, and selenium precursors simultaneously. We speculate that upon injection ZnTe cores form rapidly and preferentially due to the higher reactivity of Te with Zn to form the nuclei of small ZnTe crystals.[9] As the tellurium precursors are depleted, abundant selenium precursors competitively grow onto the existing ZnTe cores. This gradient distribution effectively produces a particular case of type II ZnTe/ZnSe core/shell QDs with extremely small ZnTe cores. The fact that these QDs are stable in air (QY 15-20%) without any further processing suggests that tellurium is fully incorporated inside the nanocrystals and not located at the QD surface. A wide FWHM of ~40 nm was observed for QDs made using the co-injection method, compared to a FWHM of 25-35 nm for QDs synthesized using the core/shell method. However, this large FWHM is expected, since precise control of ZnTe core size in individual QDs is difficult to realize using the co-injection method.

Like bare ZnTe cores, the nanocrystals produced from co-injection do not show fluorescence whereas slight addition of zinc oleate shell precursors at high temperature induces bright PL. Preliminary results also show that variation in the tellurium to selenium ratio for injection enables further tunability of the emission wavelength.

3.5 Fluorescence Lifetime Decay

3.5.1 Experimental

Photoluminescence decays were obtained by time correlated single photon counting. Hexane solutions were excited with ~50 ps 414 nm pulses at 2.5 Mhz from a diode laser, and the emission was collected through a suitable spectral filter. Single photons were detected with an avalanche photodiode module (Perkin Elmer) and their arrival times were histogrammed with a PC card (PicoQuant Timeharp 200).

3.5.2 Results and Discussions

Fluorescence lifetime decays were measured in order to explore rates of exciton recombination. Figure 3.5 shows this to be described by two processes: a fast nonexponential stage followed by a slower decay. The former one dominates and is attributed to non-radiative decay processes arising from surface defect states,[10] which is consistent with the low QY observed for this sample (~12%). The slower exponential component seemingly implies an exciton recombination lifetime of 52.5 ns but in fact this number is a lower bound of the radiative fluorescence lifetime. The relatively long lifetime (52.5 ns) suggests that electrons and holes are well separated spatially and therefore need longer time to recombine than the type I counterparts, which typically have lifetimes of around 10-20ns.[11] However, at the same time it is reasonable to

postulate that the relatively thin ZnSe shell (~0.7 nm) on a large ZnTe core (4.4 nm) leads to an incomplete spatial separation of charge carriers,[12] especially as electrons located in the thin shell have higher mobility and more tendency to delocalize and tunnel into the core.

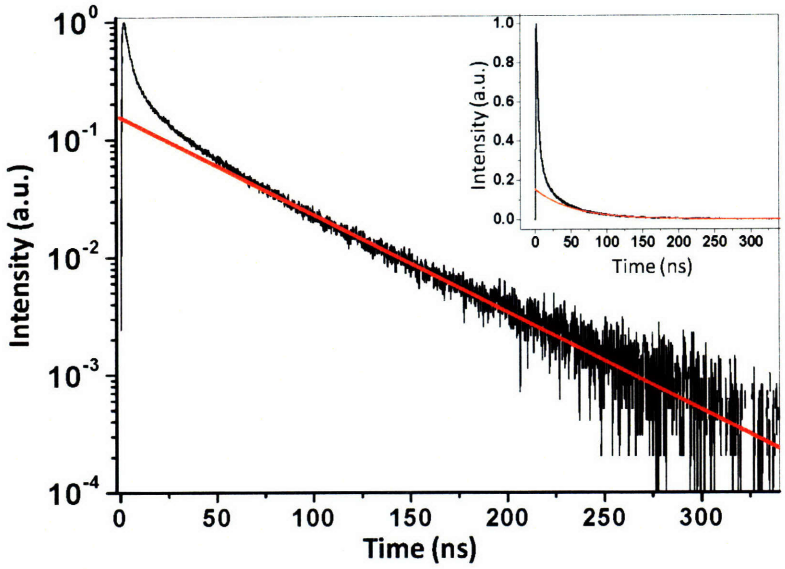

Figure 3.5 Fluorescence intensity plotted logarithmically against time lag for the same sample as in Figure 3.1D. The red curve, a fit to a single exponential in the range 77 to 340 ns, gives the lifetime of 52.5 ns. Inset: the same data (black line, data; red line, fitting) plotted on linear axes, showing that the faster nonexponential process dominated.

On the other end, we observe lifetime values very close to one another in this series of QD samples. We postulate that the difference of the thin ZnSe shell is negligible on a large ZnTe core in terms of changing lifetimes.

3.6 References

[1] U. Laheld, F. Pedersen, P. Hemmer, *Phys. Rev. B* **1995**, 52, 2697.
[2] T. Xie, X. Zhong, T. Basche, *Adv. Mater.* **2005**, 17, 2741.

[3] M. Brasil, R. Nahory, F. Turco-sandroff, H. Gilchrist, R. Martin, *J. Appl. Phys. Lett.* **1991**, 58, 2509.
[4] S. Coe, W.-K. Woo, M. Bawendi, V. Bulovic, *Nature* **2002**, 420, 800.
[5] J. Steckel, P. Snee, S. Coe-Sullivan, J. Zimmer, J. Halpert, P. Anikeeva, L. Kim, V. Bulovic, M. Bawendi, *Angew. Chem. Int. Ed.* **2006**, 45, 5796.
[6] R. Xie, U. Kolb, J. Li, T. Basche, A. Mews, *J. Am. Chem. Soc.* **2005**, 127, 7480.
[7] C.-T. Cheng, C.-Y. Chen, C.-W. Lai, W.-H. Liu, S.-C. Pu, P.-T. Chou, Y.-H. Chou, H.-T. Chiu, *J. Mater. Chem.* **2005**, 15, 3409.
[8] A. Milch, P. Tasaico, *J. Electrochem. Soc.* **1980**, 127, 884.
[9] R. E. Bailey, S. Nie, *J. Am. Chem. Soc.* **2003**, 125, 7100.
[10] P. Guyot-Sionnest, M. Hines, *Appl. Phys. Lett.* **1998**, 72, 686.
[11] H. Huang, A. Dorn, G. Nair, V. Bulovic, M. Bawendi, *Nano Lett.* **2007**, 7, 3781.
[12] S. Kumar, M. Jones, S. Lo, G. Scholes, *Small* **2007**, 3, 1633.

Chapter 4

Future Directions

As shown above, this ZnTe/ZnSe core/shell QD system is of potential interest, both from the bandgap engineering point of view and the prospects of future technical applications such as QD-LEDs.

Progress has been made, and a synthetic procedure is established. However, there are also lots of promising future directions as we now discuss.

4.1 Formation of Zinc Oxide

We observed zinc oxide species when trying to get XRD patterns for ZnTe cores. We speculate it was formed as a byproduct in the core synthesis scheme. Several XRD experiments were done to test this hypothesis.

Our initial concern that the zinc fraction of QDs being oxidized in air when we prepare and measure XRD samples does not find supports in the spectra we get. To prevent oxidation in preparing and measuring core samples, nonsolvent (methanol) precipitation and centrifugation and redispersion into solvent (hexane) was carefully performed in inert atmosphere. The process was repeated more than three times for a complete removal of residual organics. The highly concentrated QD solution was dropcast onto a zero-background silicon plate, and the plate was sealed in a vial in inert atmosphere. In addition, instead of the conventional metal lid on x-ray diffractometer, we used a special set-up which allows us to flow nitrogen through the chamber where the silicon plate sits. In this method, the only chance that the sample is exposed to air is

during the transfer of the plate from the sealed vial to the sample chamber, which is on the order of several seconds. The fact that we still see zinc oxide diffraction patterns leaves us only two possibilities: 1) The QD sample is extremely easy to be oxidized. 2) Zinc oxide is formed in the core synthesis.

Ratio of precursor seems to suggest the latter. In a typical synthesis, 1ml of 0.1 M TOP-Te and 12 mg of $ZnEt_2$ are mixed and injected into the heated flask. While we have a relatively precise control over the volume of TOP-Te solution, it is difficult to weigh the exact amount of zinc precursor given the fluctuation of atmosphere pressure in the glovebox and each drop of $ZnEt_2$ is roughly 3 mg. This effect of excess zinc precursor is easily neglected as it does not affect the PL intensity or peak positions. In one experiment, in order to test the effect of excess zinc precursor, we prepared two batches of QDs in parallel, one with 12 mg $ZnEt_2$ (A), the other with 29 mg (B), with all the rest parameters the same within experimental error. Sample B shows the ZnO differaction peaks in XRD spectrum whereas sample A lacks features of ZnO, even when we collect the signals from sample A in air for one hour (Figure 4.1). This simple experiment demonstrates that 1) ZnO is formed during the ZnTe core synthesis and 2) excess zinc precursor makes the system more likely to produce ZnO.

We note that zinc oxide peaks are relatively narrow comparing to ZnTe core signals. Knowing that larger particles give narrower peaks in XRD diffraction patterns, we filter the solution through a 0.02 um membrane after the first cycle of methanol/hexane extraction. No zinc oxide patterns are observed from the XRD spectra we get this way, further demonstrating ZnO is a byproduct of ZnTe core synthesis, and more importantly, can be easily removed from the system for future processing.

The studies on ZnO are of particular importance as we noticed sample A is much more stable in air than sample B. Originally we ascribed the poor air stability of these QDs to the oxidation of tellurium.[1] It is also reasonable to assume the air stability issue partly arises from oxidation of zinc. What we have learned here is less amount of zinc precursor is more favorable in terms of the air stability of this system.

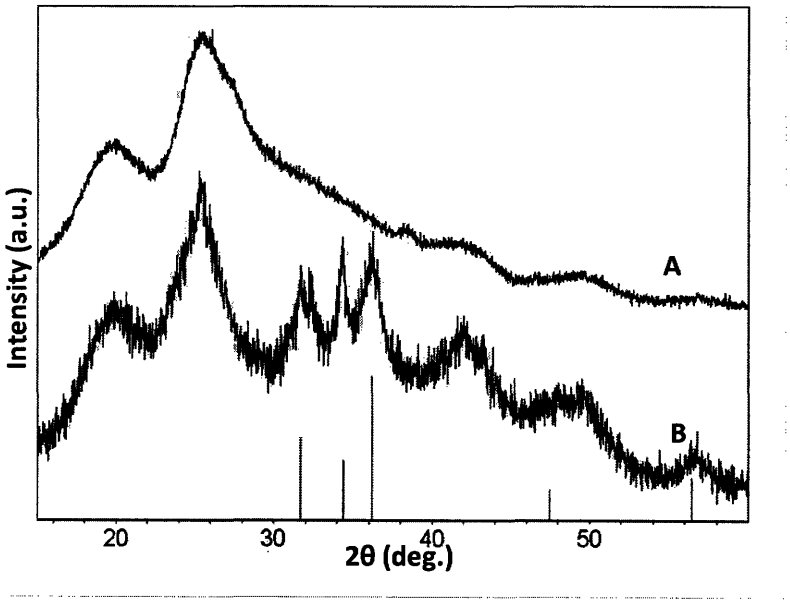

Figure 4.1 XRD spectra of ZnTe cores. A is prepared from 12 mg $ZnEt_2$ and B is synthesized from 29 mg. The marks at the bottom abscissa are the diffraction patterns correspond to bulk ZnO. While B shows diffraction patterns that are characteristic of those of bulk ZnO, sample A prepared in the same condition except the amount of zinc precursor exhibits no diffraction peaks corresponding to ZnO.

4.2 Optimization of Core Synthesis

Transmission electron microscope images show that the distribution of core size is about 13% in a typical synthesis with a 1:1 zinc: tellurium precursor ratio. In the UV-

Vis absorption spectrum for this batch of cores, the band edge absorption is not prominent as the feature is smeared out from the relatively wide size distribution.

We explored parameter space by varying the amount of tellurium precursor while the amount of zinc precursor remained the same. Figure 4.2 shows that the optimal condition for size distribution occurs around a 1:2 zinc:tellurium ratio, as we see the first absorption peak which is not seen at other conditions. We believe this has a high potential to become a robust protocol for high-quality ZnTe QD synthesis.

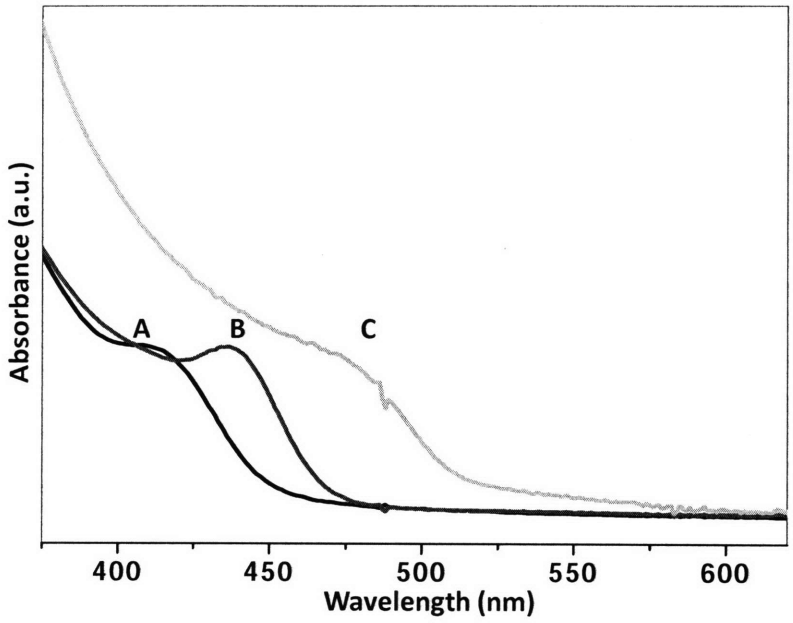

Figure 4.2 Absorption of a series of ZnTe QDs with different zinc to tellurium precursor ratio for injection when the amount of zinc precursor is fixed. A corresponds to 1:1.5 Zn:Te; B corresponds to 1:2 (Zn:Te) giving the most prominent peak feature that is not seen elsewhere; C corresponds to 1:4 for Zn:Te.

However, this 1:2 zinc:tellurium raio is not an optimized reaction condition for one-pot ZnTe/ZnSe core/shell QD synthesis. We noted in the following one-pot SILAR overcoating that the PL intensity was weak and the appearance of PL was delayed. We speculate that excess tellurium left in the pot can competitively grow into the ZnSe shell. This is especially true for high grow temperatures (240 C), long annealing times, the higher reactivity of tellurium than selenium, and the nature of a one-pot synthesis. A proposed solution is to clean up the system before the ZnSe shell growth. This clean-up can even potentially solve the tellurium oxidation problem, and will be promising if the full width at half maximum (FWHM) is narrow, which is expected from a narrow size distribution.

It is worth noting that while different ratios of precursors give different starting point for the first absorption peak position; these positions can red-shift given longer core growth time.

Multiple injections of precursors might also lead to narrower size distributions. These reaction parameters have not been adjusted yet.

4.3 Potential Solutions to the Air Stability Issue

The PL of ZnTe/ZnSe core/shell QDs is found to be quenched within a few minutes in air. From a chemical point of view, we speculate that oxidation of tellurium creates trap states and photoexcited carriers have a higher probability of falling into trap states instead of undergoing radiative recombination.

A proposed solution is to overcoat core/shell QDs with a protective layer (such as ZnS or ZnSe). We find one-pot overcoating alleviates the PL quenching problem, but

does not solve it. This implies that tellurium is at the surface of the nanocrystals. When we consider the source of tellurium at surface, two possibilities need to be taken into account: 1) excess tellurium left from the one-pot synthesis being incorporated into the shell; 2) tellurium in the core region diffuses out to the surface. The fact that tellurium atoms are big and should be well confined within their crystal lattice leads us to believe that the first source is more likely.

In order to remove excess tellurium from the growth solution, methanol/butanol/hexane extraction of growth solution is performed in inert atmosphere. The QD solution in hexane is then transferred into a flask containing previously degassed solvents (oleylamine and octadecene) at 60 C. The PL diminishes after a few minutes in the flask and is not recovered after overcoating a layer of ZnSe or ZnS. However, slight addition of zinc oleate to the flask before PL diminishes is found to keep the PL intensity intact, even when the solution is heated up to 120 C. The details are not precisely known. What we believe now is that the non-solvent extraction removes organic ligands from the surface of the nanocrystals to the point that slight heating quenches the PL completely. Addition of zinc oleate can fill the vacancies from the removed organic ligands and passivate the surface of the nanocrystals.

After the PL is retained, two alternative ways to overcoat these ZnTe/ZnSe core/shell dots are explored.[2, 3] Both methods start with the same solvent system (1 ml oleylamine and 3 ml octadecene) while they differ in the precursor choices and reaction conditions. One method is to mix zinc oleate and TOP-S (1:1 in ratio) in TOP, and add to the pot at a rate of 1 ml/hr at 190 C. A few hours' annealing after the complete addition usually increases PL intensity. Another method is to mix $ZnEt_2$ and $(TMS)_2S$ in TOP,

and add to to the pot at a rate of 1 ml/hr at 150 C. The processed QDs are found to be stable in air up to periods of months. Note the precursor pair is not exchangeable. In different trials, we tested the combination of zinc oleate and $(TMS)_2S$. The PL intensity was found to be significantly enhanced at first, but quenched shortly afterwards. We ascribe this to the much higher reactivity of $(TMS)_2S$ compared to zinc oleate and the shell tends to become sulfur-rich. This imbalance in chemical composition likely quenched the PL.

To be thorough, we also tested the air stability of QD powders after we perform methanol extraction on these overcoated QDs. The PL of these QDs in solid form is found to be quenched after a few minutes in air. If we redisperse these QDs in hexane and add either zinc oleate or TOP, the PL can be retained for months.

In addition, a control experiment was done by adding Br_2 in water on these overcoated QDs. As a strong oxidant, Br_2 should easily oxidize tellurium. In this experiment, we observe immediate quench of PL, which suggests that oxidation of tellurium is the cause of air stability issues.

Later TEM images show that for QDs fluoresce at wavelength 560 to 590nm, the shape of the nanocrystals is not spherical. Instead, prism-shaped dots comprise a large fraction of the sample. Bearing in mind the intrinsic lattice mismatch between ZnTe and ZnSe (8%), we know it is difficult to grow thick shells even when one carefully uses high growth temperatures and long annealing times. The problem might be worse with ZnS, which has a even larger lattice mismatch with ZnTe. In our experiments, we start with dots that show PL around 545 nm, which we now believe is roughly 4.4 nm in core size

and 0.7 nm in shell thickness (with an overall size of 5.8 nm). On the other hand, QDs that show PL below 545 nm can be spherical. A proposed solution is to start with a smaller ZnTe core, and a thinner ZnSe shell. In that case, with a new thick shell overcoated on top of this core/shell construct, air stability issues might be finally resolved.

4.4 Further Tunability

As demonstrated earlier, these ZnTe/ZnSe core/shell QDs have PL from 480 nm to 590 nm. According to quantum confinement effects, if we start with bigger ZnTe cores, and grow thick shells on the existing cores, we should be able to tune the PL to the red of 590 nm.[4]

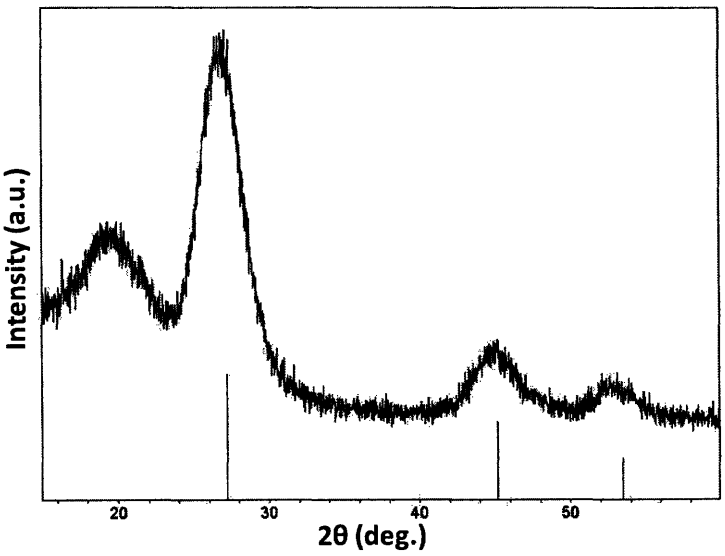

Figure 4.3 XRD pattern from a sample made simultaneous co-injection of zinc, tellurium, and selenium precursors. The marks on the bottom abscissa are peaks characteristic of those for bulk ZnSe (zinc blende).

To access PL below 500 nm, we attempted the co-injection method. Preliminary results show that by varying the tellurium to selenium ratio, the PL can be tuned from 430 nm to 500 nm. Some characterizations are done. Here we give an example where we start with a 15:85 tellurium:selenium ratio for co-injection. Figure 4.3 is the XRD pattern of the co-injection QDs. The peaks are slightly shifted from ZnSe (zinc blende) towards ZnTe (zinc blende) while the sample largely exhibits the characteristic diffraction pattern of ZnSe. This is expected as selenium dominates in precursor composition. Wavelength dispersive x-ray spectroscopy shows the core composition after the co-injection as Zn, 55%; Se, 42%; Te, 3%. We can see selenium is dominating in the anion composition. TEM images reveal the size is about 3.7 nm (Figure 4.4). The superlattice structure suggests that high crystallinity is achieved in this method. PL lifetime decay was measured to further characterize these co-injection QDs. The lifetime for this sample is about 50 ns (Figure 4.5). The relatively long lifetime suggests that carriers are spatially separately even when the core is small.[5]

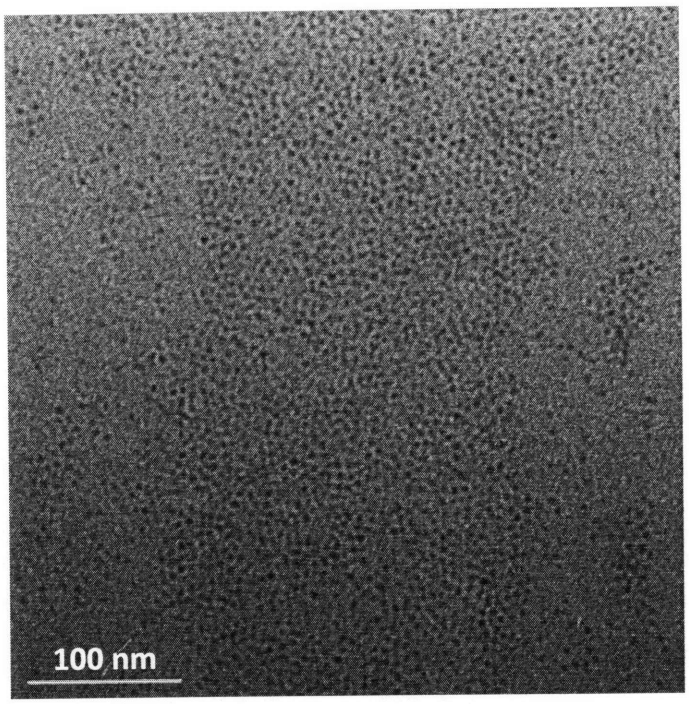

Figure 4.4 Transmission electron microscopy image of QDs produced by co-injection method.

The system is potentially interesting not just because of its tunability, but also for its air stability, and for high quantum yields. Samples prepared by the co-injection method are stable in air without further processing. We believe tellurium atoms have a high reactivity and bind to zinc atoms to form small cores before selenium atoms can do so. As the tellurium precursor is depleted, selenium precursors and excess zinc precursors grow onto existing ZnTe cores. This effectively creates a ZnTe/ZnSe core/shell structure with an extremely small ZnTe core. Or this construct can be seen as tellurium center-doped ZnSe QDs. Without tellurium on the surface of the nanocrystals, the air stability issue is minimized. The quantum yield in the co-injection method is typically around 25%, better than their core/shell counterpart (15%).

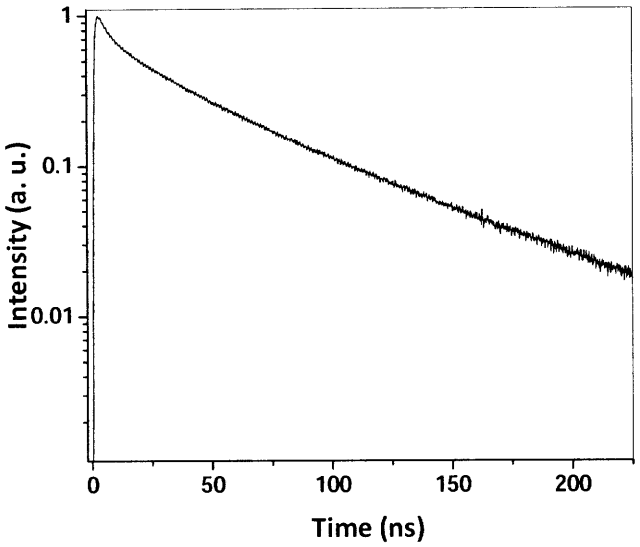

Figure 4.5 fluorescence intensity decay plotted logarithmically against time for QD samples produced in co-injection method. The lifetime measured is typically on a scale of 50 ns.

A large FWHM (~40 nm) is observed for this co-injection QD sample whereas its core/shell counterpart has a typical FWHM of 25 – 35 nm for PL below 550 nm. This large FWHM is expected as the precise control over elemental distribution in individual QDs is difficult to realize.

4.5 Conclusions

In summary, there are lots of important future directions arising from this ZnTe/ZnSe core/shell system. For one thing, addressing the air stability issue, different reaction schemes are proposed such as the precursor usage, the purification and overcoating method. For the other, the co-injection method produce high-quality air-stable QDs and these QDs can be tuned over a wider range by changing reaction parameters.

4.6 References

[1] A. Milch, P. Tasaico, *J. Electrochem. Soc.* **1980**, 127, 884.
[2] R. Xie, U. Kolb, J. Li, T. Basche, A. Mews, *J. Am. Chem. Soc.* **2005**, 127, 7480.
[3] C.-T. Cheng, C.-Y. Chen, C.-W. Lai, W.-H. Liu, S.-C. Pu, P.-T. Chou, Y.-H. Chou, H.-T. Chiu, *J. Mater. Chem.* **2005**, 15, 3409.
[4] T. Xie, X. Zhong, T. Basche, *Adv. Mater.* **2005**, 17, 2741.
[5] H. Huang, A. Dorn, G. Nair, V. Bulovic, M. Bawendi, *Nano Lett.* **2007**, 7, 3781.

Appendix I

As the successor of Brian Yen, I have also been working on the microfluidic reactor project. There are mistakes made, experiences gained. I summarize them here for possible future reference.

A great improvement is to employ compression parts, instead of the conventional tubing and sealing method. Compression parts can stand high pressure, and are reusable so that no more effort needs to be spent on sealing steps in fabrication once the reactor part is done.

Details in fabrication

To speed up the process, there are a few steps we modified from Brian's standard procedures.

1) No need to grow oxide in between each step.

Growing oxide in tube A2 generally takes ~ 8 hours, and the cleaning up in the preparation stage is stringent and time-consuming. The procedure we start with including growing oxide after each etching step, which is sometimes unnecessary. In the current process flow, for each reactor, we only use tube A2 once, before we do the anodic bonding. The reactors we fabricated this way are of high quality, and can withstand pressures as high as 60 bar.

2) No need to bake wafers in between sides.

In most cases, double-side coating is necessary. The conventional procedure is to first coat one side, bake for one hour, and then coat the other side, and bake again for one hour. What we found feasible is to coat the first side, bake for 5-10 min (just to remove solvent), then coat the other side, and bake for half an hour before UV exposure.

3) No need to immerse in acetone for 6 hour.

In STS silicon through-etching, we need to mount the silicon wafer to a quartz wafer beforehand. After the process, a usual procedure is to immerse the wafer in acetone for six hours to dissolve adhesive photoresist. Experimentally, we found sonicating the wafer in acetone for 10 min is sufficient to separate the silicon wafer and quartz wafer, and therefore greatly speed up the process.

4) Acid hood 2 is faster than acid hood 1.

When you can, get trained on acid hood 2 after you are qualified for acid hood 1. The rate-limiting step in acid-hood is the cleaning up afterwards. Acid hood 2 has an advantage in that.

5) Wait until helium leakage check is done on STS.

Obviously, I learned this from a previous mistake made. Helium leakage check is a critical step in STS silicon etching. After this step, the plasma etching will start and go on for a designated period of time so that you can go back to the wet-lab and do more work. However, if for some reason, the leakage check is not able to complete, the whole process is on hold. You come back five hours later, only to find your fabrication schedule is messed up.

6) Booking equipment

Try to qualify as a 24 hour user. Besides that, EV1 is a heavily used apparatus. So when planning the fabrication, try to find the slots for EV1, and work things around that.

Appendix II

A few interesting directions for in microfluidic reactors:

1) Heterogeneous structure.

One example is ZnTe/ZnSe core/shell tunable system. By feeding different amounts of precursors or employing different residence times, one might be able to demonstrate in a straightforward way the tunability of that system.

Grow rod-like shell structure. The essential idea of the design is to keep the concentration high, and thus the growth becomes more anisotropic and less spherical. By feeding precursors into side channel, one can easily maintain a high concentration. For a model system of CdSe/CdS core/rod-like shell, once the condition is optimized in batch mode, it should be easy to adapt into microfluidic reactors. A possible modification is to grow an alloy shell to form CdSe/CdZnS particles.

2) Characterization of supercritical fluid.

Recently, we found supercritical hexane a suitable medium to grow CdSe quantum dots. The product is of high quality with narrow size distribution. We need to design a model reactor and find a suitable probe to characterize that system.

3) In-line monitoring system.

To build an in-line monitoring set-up is one of the goals in the future. With a rapid detection of absorption and photoluminescence, the efficiency of screening over a wide range of reaction parameter should be greatly increased.

Acknowledgement

I cannot express how thankful and lucky I feel to have spent time in our Bawendi family. Every one of you has been very helpful and supportive throughout. It is from all of you that I learned English, quantum dots, and many other important things in life.

Thank you, Moungi, for generously deciding to take me into this family a year and a half ago. It has been a wonderful journey with you! I have learned so much from you. Your broad and solid knowledge background gives me strong support for what I have achieved today, and your patience makes me feel grateful. And, your sense of humor (especially when it is unintentional) leaves a big impression on me. You changed my entire life. Without you, I cannot imagine what I would be like today.

Thanks to everyone else here! Hao, cannot say enough "thanks" for your strong support and encouragement throughout. My officemates... Scott, thank you for eating all my cookies (without my permission) and constantly checking my lab notebook (I still owe you "The Beast."). And, I will not forget the happy days when we moved giant liquid nitrogen tanks underground, the times when you showed me how to do crashout, how to measure quantum yields, how to... Gautham, thanks for teaching me "Elite Beat", introducing a few interesting books, and helping with the lifetime data part of this work. Thanks for creating "Juan" as a unit of silliness – I am flattered! Jon, I enjoyed myself so much practicing Chinese with you, and enjoyed learning things like "ravioli". And, for all the overcoating work I have done, I give unreserved credit to you, for teaching me that, and for cleaning up the mess at centrifuge machine for me when I made that stupid mistake. Lisa, thanks for answering all my stupid questions, and I like your company at my hood!

Thank you, Binil, for all those helpful discussions on research and many other things in life. I am honored to have you as a hood neighbor. Thanks for putting up with my incessant borrowing stuffs from you. Cliff, I am especially grateful for your help on TEM. I also greatly enjoyed the stupid club we used to go together, and all the meals and ideas we shared. Juwell, I like the joys you brought to me. Your jokes kept me awake at 3 am and on boring Sundays. Your fighting experiences with tellurium benefited me in a way you would never know. Jongnam, I appreciate the nutrient food for group meetings. You taught me everything I need to know when I knew nothing. That meant a lot to me! Wen, thanks for always being patient and kind to me, teaching me every little thing such as keeping a lab notebook, changing pump oil, doing DLS measurement, and so on. In the future, no one will pretend that he/she wants to punch me, and I will miss that a lot. Numpon, I enjoyed chatting with you every day in the wet lab, and learning Thai from you. Thanks for teaching me many useful lab techniques. Thank you, August, for sharing the frustration at clean rooms. The stories and jokes you told broadened my horizon.

My "first-year" buddies Brian, Peter, and Hee-Sun... Without you, I wouldn't make it. Brian, I will always cherish the mornings we walked together to the lab, and the late nights we spent chatting in office when no one else was around. Peter, thanks for all your help and encouragement throughout. Thanks for all the good ideas, the culture lessons,

the news we shared from biased broadcasting corporation... Hee-Sun, I will treasure all the meals we shared/cooked together, and all the good advices you gave me.

Sam, for teaching me every skill I need at clean rooms, tolerating every stupid mistake I made, and transforming me to a competent fab user and an engineer. Thanks for all the coffee you bought me. Venda, you patiently taught me the standard procedures of quantum dots synthesis, from which I am still benefiting today. Dave, I am so fortunate to have inherited all my lab equipment from you. They are great tools! Becky and Andrew, you both gave me tremendous help in the wet lab. Li, your kind assistance made my life a lot easier. Thank you all!!